Transactions, **SMiRT-26**
Berlin/Potsdam, Germany, July 10-15, 2022
Special Session

DISCUSSION OF PHENOMENA AND COMPUTATIONAL MODELING FOR FLOW THROUGH STEAM GENERATOR TUBE LEAKS

Klaus Heckmann[1], Jürgen Sievers[2], Fabian Silber[3], Stefan Weihe[4]

[1] Technical Expert, GRS, Cologne, Germany (klaus.heckmann@grs.de)
[2] Chief Expert Structure Mechanics, GRS, Cologne, Germany
[3] Research Scientist, MPA University of Stuttgart, Germany
[4] Managing Director, MPA University of Stuttgart, Germany

ABSTRACT

Steam Generator Tubes (SGT) are the thinnest component of the Reactor Coolant Pressure Boundary (RCPB) of a pressurized water reactor. A local leak in one of these tubes will lead to a flow to the secondary side with lower pressure. As the wall of the SGT is much smaller than the walls of other components of the RCPB, the flow description differs significantly from the well investigated mass flow through leaks in thicker walls, which has an impact on the phase change and the mass flow rate, motivating recent research. This paper summarizes computational approaches for describing "gate-like" leaks in SGT with a jet of metastable liquid water and compares it to incompressible flow and two-phase flow established for "tunnel-like" leaks. The model predictions are compared to mass flow rate measurements and optical characterizations at the exterior side of the leak. In addition, the observed back pressure effect is discussed and the importance of crack morphology for the detectability assessment is highlighted.

INTRODUCTION

The understanding of phenomena related to leaks in steam generator tubes (SGT) gained significant importance in the recent years. These efforts are supported by experimental investigations, see e.g. Revankar and Riznic (2019), Zhang et al. (2019), Zhang et al. (2020), and Silber et al. (2021) for most recent publications. With these insights gained from laboratory tests of specimens in thin plates or actual steam generator tubes, it is possible to improve the modelling and to allow an improved computational prediction of the mass flow rate through an SGT leak (Heckmann et al., 2022).

Leak rate prediction and the assessment of model accuracy is a well-studied field in nuclear technology, see e.g. Schmid et al. (2021) for a recent paper. However, in many investigations the leak-before-break relevant case of highly reliable piping of Reactor Coolant Pressure Boundary (RCPB) with thick walls was in the focus. Hence the component geometry for SGT leaks differ a lot from the majority of leak rate investigation, and also other circumstances render the SGT case unique (see Table 1). It was pointed out by Heckmann and Sievers (2018) that also in the modelling of such leak, significant differences have to be explained.

Table 1. Comparison of "typical" properties for thick-wall pipe leaks and SGT leaks

		Thick	SGT
Pipe diameter	[mm]	200-800	22
Wall thickness	[mm]	30-70	1-1.2
Back pressure	[MPa]	0.1	5.5
Detection threshold	[g/s]	63	1

This paper is organized as follows. In the first section, the flow pattern and the approach of a metastable jet is discussed and compared with experiments. In the section thereafter, the back pressure effect is discussed and experiments are analyzed. The third technical section is dedicated to morphology effects. The paper concludes with a summary section.

FLOW PATTERN AND METASTABLE LIQUID JET APPROACH

The most significant phenomenon potentially present in SGT leaks but usually not in thick-wall pipe leaks is the delay of evaporation. Due to the rapid decompression of the fluid passing the short path of wall thickness, the pressure can drop significantly below the saturation pressure without vapour formation (or with reduced vapour formation, compared to equilibrium thermodynamics). This was observed for Freon flow through short nozzles by Fauske and Min (1963), and consequently Zaloudek (1963) indicated that a jet of metastable liquid is the flow pattern in this region. The instant phase transition of this jet afterwards is also known as flashing, see Liao and Lucas (2021) for a recent review. This phenomenon will be in the focus of the computational modelling in this paper.

Modelling

The aim of modelling within this paper is restricted to a 0-dimensional or 1-dimensional (0D/1D) model: The fluid motion is considered along one axis from interior side to exterior side (1D) or as a relation of the two volume conditions (0D). In accordance with Zaloudek (1963), three different patterns can be identified in the RCPB and SGT leaks: A stationary 2-phase flow, a metastable liquid, and an incompressible liquid flow. This situation is shown in Figure 1.

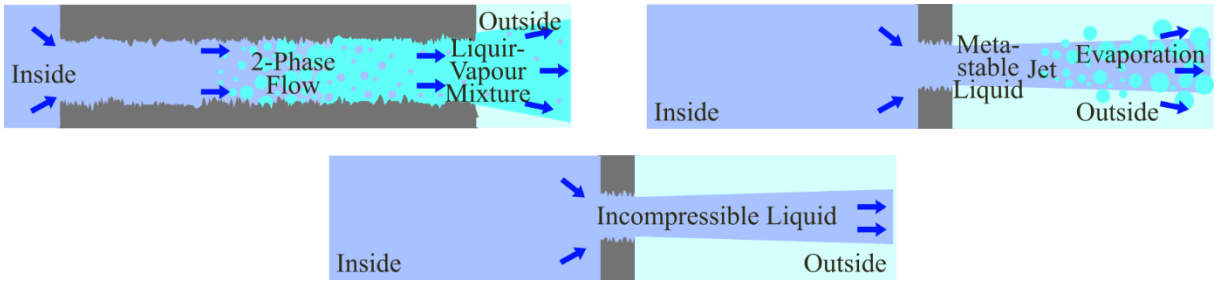

Figure 1. Flow pattern schemes for the 0D/1D models

The simplest situation is the incompressible fluid of density ρ, which is expected for cold water at the interior side. The mass flow rate $\dot{m}$ (or alternatively, the flux density G) is described by the Bernoulli equation.

$$\dot{m} = A\, c_d \sqrt{2\rho(p_{in} - p_{ex})} = A \sqrt{\frac{2\rho(p_{in} - p_{ex})}{1+\zeta}} = A\, G \qquad (1)$$

In this case, the mass flow rate is proportional to the square root of the pressure difference between inside and outside. Besides the leak cross section A, the discharge coefficient $c_d < 1$ (or alternatively, the resistance $\zeta > 0$) describes the reduction of the flow due to form losses, effective cross section reductions or friction.

A generalization of the incompressible fluid motion is the adiabatic subcritical flow of a single-phase compressible fluid. In this case, the flow rate is driven by the difference in the specific enthalpy h between interior side and exterior side.

$$\dot{m} = A\, c_d\, \rho_{ex} \sqrt{2(h_{in} - h_{ex})} \qquad (2)$$

This is the basis for the metastable jet model proposed by Heckmann et al. (2022), with assuming the properties of metastable liquid water at the exterior conditions. This corresponds to an exterior side density of $\rho_{ex} = \rho_L(s_{in}, p_{ex} < p_{sat})$ and similar expression for the enthalpy; the properties of water have to be extrapolated from equilibrium steam tables. The assumption of this model is that the flashing starts not in the leak channel, but downstream in the free jet on the exterior side.

The situation becomes more complicated if evaporation takes place in the leak and affects the leak flow rate. Out of the several existent approaches for this situation, the Pana model is selected for discussion here, see Pana and Müller (1978). One main reason for this choice is that the Pana model is also well-defined for single-phase flow in the limit of low temperature. The compact form of the mass flux density G is given in Eq. (3).

$$G(p_0, s_0, \zeta, p_{ex}) = \max_{p_1} \left[\max_{k} G_{\mathrm{Moody}}(k, p_1) \right]_{p_2(p_1) > p_{ex}} \qquad (3)$$

The inner function is the Moody flux density with a slip parameter k, where the parameter $p_1 \leq p_{in}$ corresponds to the pressure in the leak after entering but before friction effects start.

$$G_{\mathrm{Moody}}(k, p_1) = \sqrt{\frac{2\,(h_0 - (1-x)h_L - x\,h_G)}{[x\,v_G + k(1-x)v_F]^2 \left(x + \frac{1-x}{k^2}\right)}} \qquad (4)$$

The outer maximization in Eq. (3) varies the entrance pressure p_1 with the side condition that the total resistance ζ is consistent with the drop from p_1 to the exit pressure drop $p_2 \geq p_{ex}$.

$$\zeta = -2 \int_{p_1}^{p_2} \frac{1 + G^2 \left(\frac{\partial v(p)}{\partial p}\right)_s}{G^2 v(p)}\, dp \qquad (5)$$

In this equation, $v = 1/\rho$ denotes the specific volume of the equilibrium liquid-vapour-mixture. Of course, the exit pressure p_2 cannot drop below the exterior side pressure p_{ex}, but typically the exit plane pressure is well above.

Finally, the criticality of the flow (in the sense of the sensitivity of the flow to the exit pressure) can be discussed by these three formulae. The incompressible fluid approach is clearly subcritical, and this approach should be valid up to $u < c_s$, where c_s is the speed of sound and $u = G/\rho$ is the velocity. The situation is similar for the compressible liquid flow (metastable jet approach), but it should be mentioned that the existence of the metastable phase is restricted to the spinodal region: The metastable phase does not exist beyond a certain region of the phase diagram. The 2-phase flow is typically critical since the flow rate does not depend on p_{ex} as long as $p_{ex} < p_2$.

Remarks On The Graphical Evaluation Of Leak Rate Experiments

The preceding subsection summarized three alternative approaches which predict, in principle, the leak rate for a single experimental leak setup. For such a test specimen of given cross section A and resistance specification c_d or ζ three different relations result for the flow rate as a function of temperature and pressure. At the same time all three models should agree on the incompressible fluid flow as the low-temperature limit. Therefore, the focus of comparison of leak rate experiments with the model prediction should be on the variation of the mass flow rate as pressure and temperature change.

The comparison therefore involves the comparison of three prediction values with one reference value, as a function of two parameters (pressure p and temperature T) which are also important to be interpreted with respect to saturation conditions. As this is challenging to represent graphically, a few alternatives are discussed in the following. As an example, the specimen VS055 described in Heckmann et al. (2022) is selected.

One option is the 3-dimensional representation (left graph of Figure 2) of the flow rate as a function of pressure and temperature on separate axes. The downside of this option is the difficult visual comparison of the models and measurements at single measurement points. Alternatively, a traditional option of model deviation assessment is the graph of predicted vs. measured values (right graph of Figure 2), but the crucial information about the fluid conditions is entirely lost in this representation.

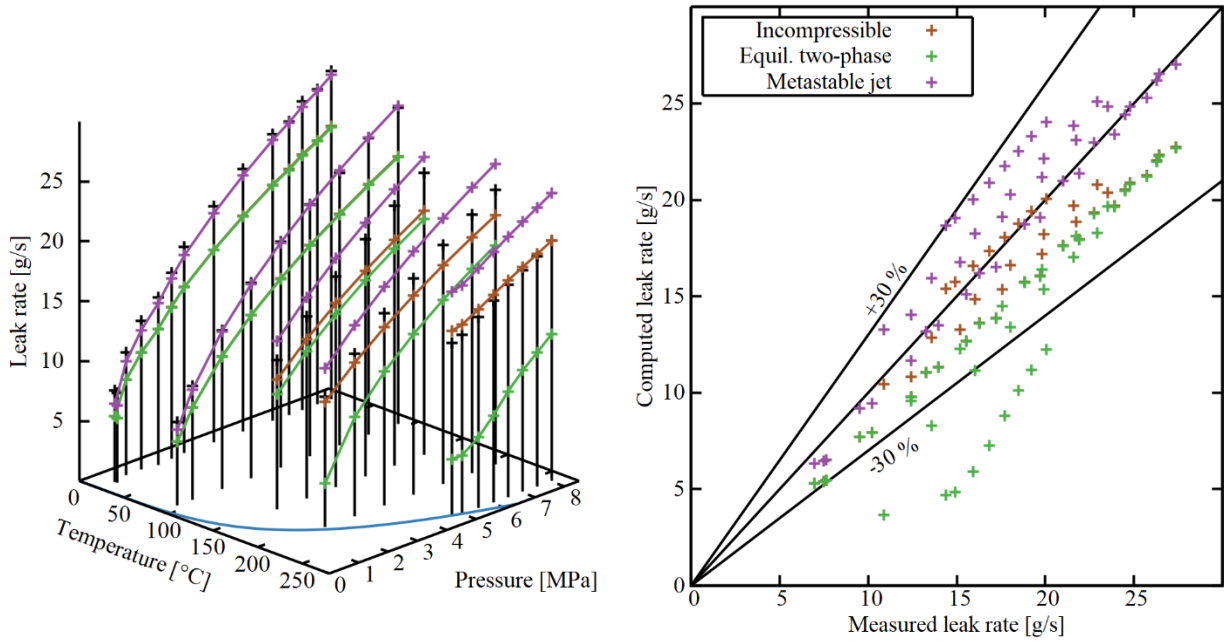

Figure 2. Leak rate experiment evaluation as 3-dimensional representation (left) and model deviation (right)

Another option is available if the points in the pT-plane are ordered to specific levels, at least in one coordinate. This is the case for the selected experiment; the temperatures are approximately equal to five different temperature levels. Although the full thermodynamic information is now contained in Figure 3, the diagram is harder to understand the more temperature levels exist. An alternative is to number the measurement points consecutively and to provide the position of the individual tests in a pT-diagram. The leak rate as a function of the test number can be compared in a separate graph. This option turned out to be very useful (left graph in Figure 4) in case of many different leak rates to compare and few thermodynamic conditions.

For the computation of a test series with really many points, it turned out effective to use a second graph joined to the leak rate vs. test number diagram, to track the temperature and pressure change. To concentrate the information, both parameters are shown in the same diagram with color-coded axes; the saturation conditions are shown as dashed lines. This leak rate experiment analysis diagram will be used in the next subsection.

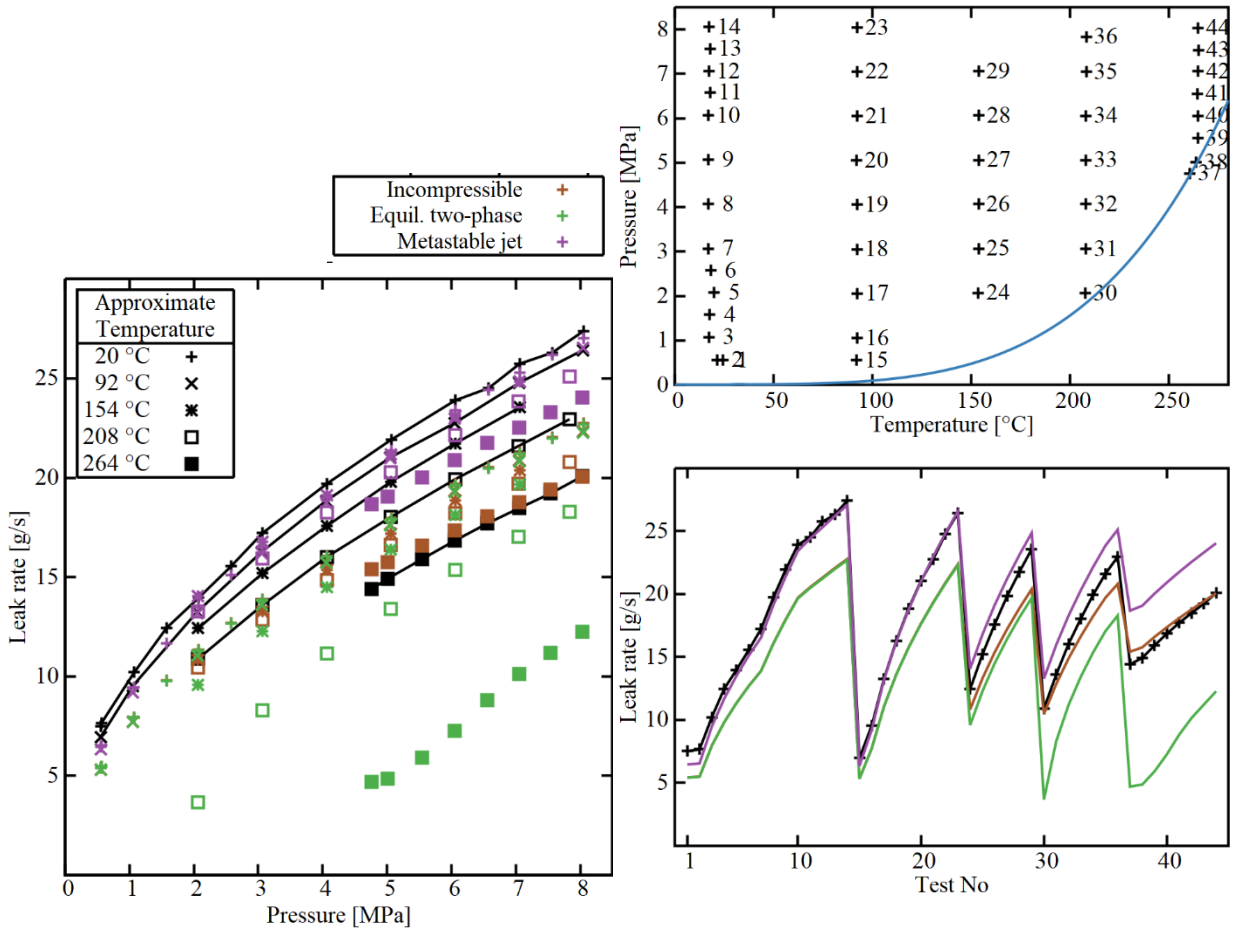

Figure 3. Leak rate experiment evaluation as pressure-dependence for different temperature levels (left) and with test number assignment in a pT-diagram (right)

Gate-like leaks vs. tunnel-like leaks: Mass flow rate

The characteristics that is responsible for the formation of either a stationary two-phase flow or a metastable jet is generally assumed to be the ratio of flow length to hydraulic diameter (wall thickness), L/d_h. The hydraulic diameter characterizes the leak cross section and is defined as four times of the ratio of cross section area to perimeter; it generalizes the diameter of circular tubings. While for large L/d_h (long relative flow paths) a stationary two-phase flow is expected, the metastable jet flow pattern is expected for small L/d_h. As an illustration of these two cases, the small L/d_h ratios belong to “gate-like” leaks, while the large L/d_h ratios belong to tunnel-like leaks.

From the available experiments, two cases are selected for the comparison of the models with the tests. The specimen VS055 has a circular hold with a diameter of about 626 µm inside and 592 µm outside in a plate of 1.2 mm thickness. The specimen R6 is a fatigue crack in a 1.3 mm thick plate with an area of 2.1 mm² inside and 3.5 mm² outside, with hydraulic diameters of 100 µm and 156 µm, respectively. and (both are also described by Heckmann et al., 2022). The leak rate experiment analysis diagrams of both specimens are shown in Figure 6.

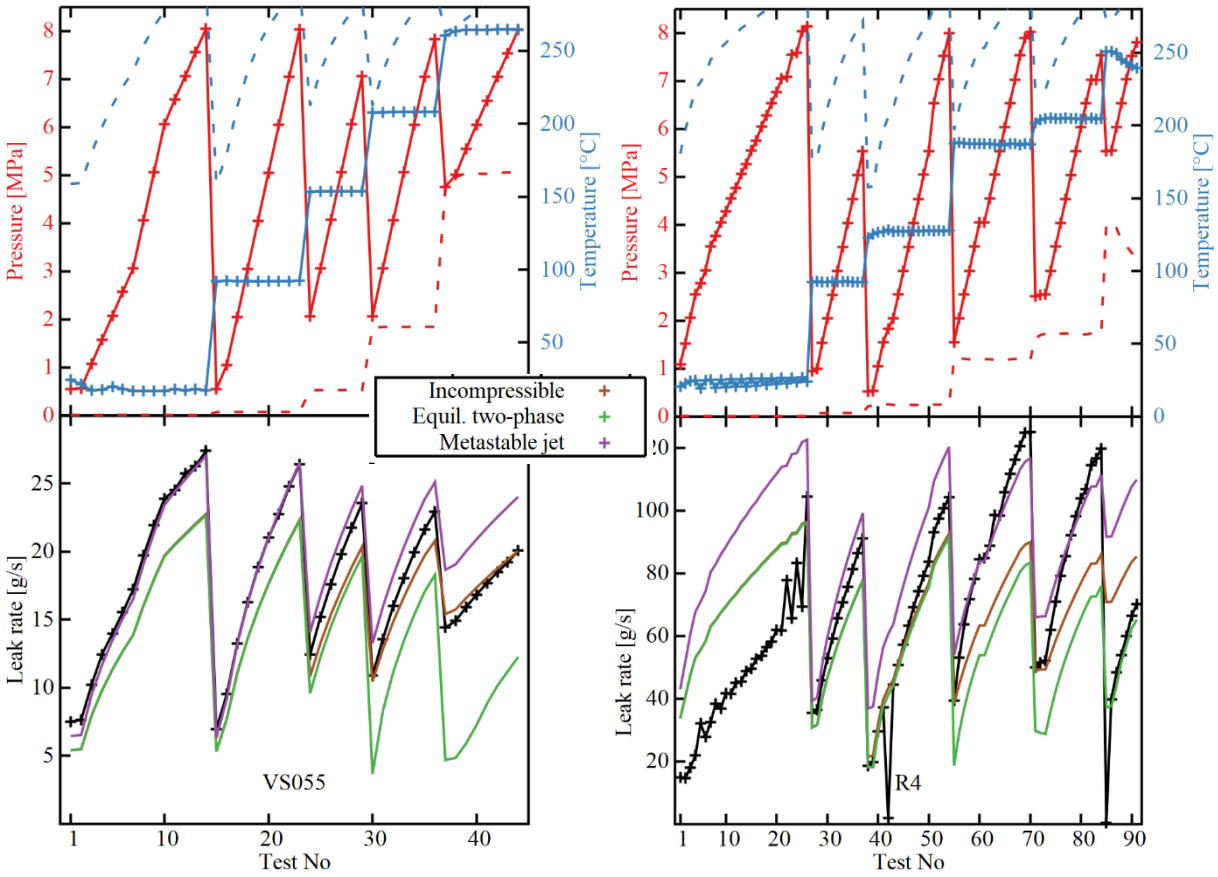

Figure 4. Leak rate experiment analysis diagrams of VS055 (left) and R4 (right).

In this diagram, it is visible that the solutions agree for the cold-water tests (although there is some irregularity observed in the first measurements of the R4 test, which could be related to effects from the start-up of the test facility). On the highest temperature levels of the gate-like specimen VS055, the two-phase solution develops an important under-estimating trend, while the incompressible single-phase solution is overestimating. The metastable jet solution is between the two. In case of the tunnel-like specimen R4, this is different: The metastable jet solution is overestimating the actually measured flow rates, and the two-phase flow solution provides a good description of the flow rates. This observation is in accordance with the expectation that a metastable jet is formed for the gate-like specimen VS055 and a two-phase flow pattern is formed in the tunnel-like specimen R4. Note that the absolute accuracy of the models varies in detail, but the proposed leak rate experiment analysis diagram allows to assess the crucial pT-dependence of model predictions and measurements.

Optical measurement of the exit flow pattern

Another opportunity to verify the model assumption is the characterization of the exit flow pattern. This type of measurement can be realized with optical cameras. Heckmann et al. (2022) describe this approach; a selection of flow pattern is presented in the following. Besides the specimen VS055 representing a gate-like leak, the specimen VS060 with a 640 µm circular hole in an 8 mm-plate is chosen. At an interior pressure of 5 MPa, four temperature levels are chosen. The photographs of the exit flow patterns are shown in Figure 5 (note that the temperatures for both specimens are slightly different for two cases, which is indicated in parenthesis).

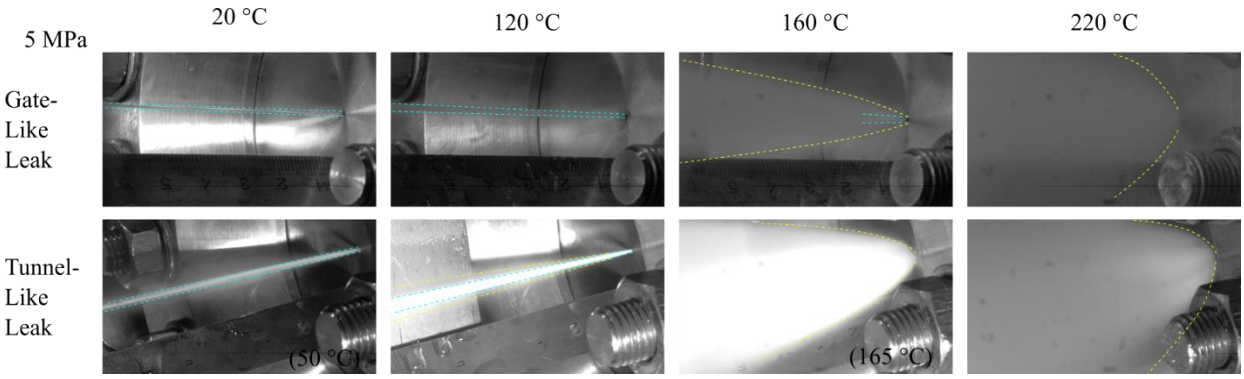

Figure 5. Optical measurement of the exit side flow pattern for VS055 (upper row) and VS060 (lower row), with indications of jet (blue) and steam cone (yellow)..

At room temperature, a liquid jet is observed for the gate-like leak and the tunnel-like leak. At 120 °C, some steam is observed for the tunnel-like specimen, while no steam could be identified for the gate-like specimen. At 160 °C, the side of the tunnel-like specimen is covered by a steam cloud, whereas for the gate-like specimen the liquid jet surrounded by steam can be observed. At 220 °C, only a steam cone is visible for both specimens.

On should mention that this observation of exit flow pattern has a certain relation to the inside flow pattern relevant for the computational modelling, but it is not a direct measurement. For instance, the observation of a significant steam content at the exit side may indicate that a two-phase flow with a large volumetric steam content is established inside the leak, but it can also originate from flashing metastable liquid directly outside of the leak. The relation between inside flow pattern and exit side flow pattern is compared in Table 2.

Table 2. Flow pattern inside the leak and observable patterns at the exit

Inside Exit side	Liquid jet	Jet & steam	Steam cone
Single phase	Possible	No	No
Metastable jet	Possible	Possible	Possible
Two phase	No	Possible	Possible

In this sense, the metastable jet approach offers an explanation that is consistent with the expectations and the observation, although it is not directly verified by the optical measurements. However, the two remarkable points are that there is a difference between gate-like leaks and tunnel-like leaks regarding the pT-dependence of the flow pattern (similar as for the mass flow rate), and that also for gate-like leaks vapour formation can be observed (in contrast to the observation from Fauske and Min, 1963, with Freon and also in contrast with expectation from single-phase discharge assumptions for SGT).

SECONDARY SIDE CONDITIONS AND BACK PRESSURE EFFECT

The second important different of SGT leak compared with RCPB-to-containment leaks is the secondary side conditions. Heckmann et al. (2022) investigated tests with cold water at atmospheric conditions at the exterior side, reporting that no effect on the flow rate is observed, compared to air environment. Zhang et al. (2019) and Zhang et al. (2020) investigated the flow rate of cold water through SGT-like specimens for different pressure levels at the exterior side; they observed that the mass flow rate depends only for smaller pressure differences on the exterior pressure and is independent for higher pressure. This resembles the

phenomenon of critical flow, but this is unexpected for cold water discharge at the investigated pressure range.

As an analysis example here, the Tube Slit 3 specimen results published by Zhang et al. (2019) is selected. The slit has a length of 3 mm and a width of 0.13 mm. These dimensions allow to compute the flux density G and the fluid velocity $u = G/A$, and consequently the Mach number u/c_s and the Reynolds number Re.

$$Re = \frac{u\,\mathrm{COD}\,\rho}{\eta} \qquad (6)$$

With cold water values of density of 997 kg/m³ and a viscosity of 0.001 Pa s is considered. The speed of sound in cold water c_s of 1480 m/s is used. Using the incompressible single-phase flow equation (1) expected for cold water flow, it is possible to compute the effective back pressure; by doing this, a discharge coefficient of $c_d = 0.85$ was selected which gives a reasonable result in the range where $\dot{m}$ depends on the exit pressure. In Figure 6, the nominal and the computed exterior pressures are shown as a function of the exterior pressure, to indicate the increasing discrepancy between these two values and also the minimal effective exterior pressure. As either transitions from laminar/transitional to turbulent flow or critical flow related to the speed of sound are expected as explanations, the computed Mach number and the computed Reynolds number are also depicted.

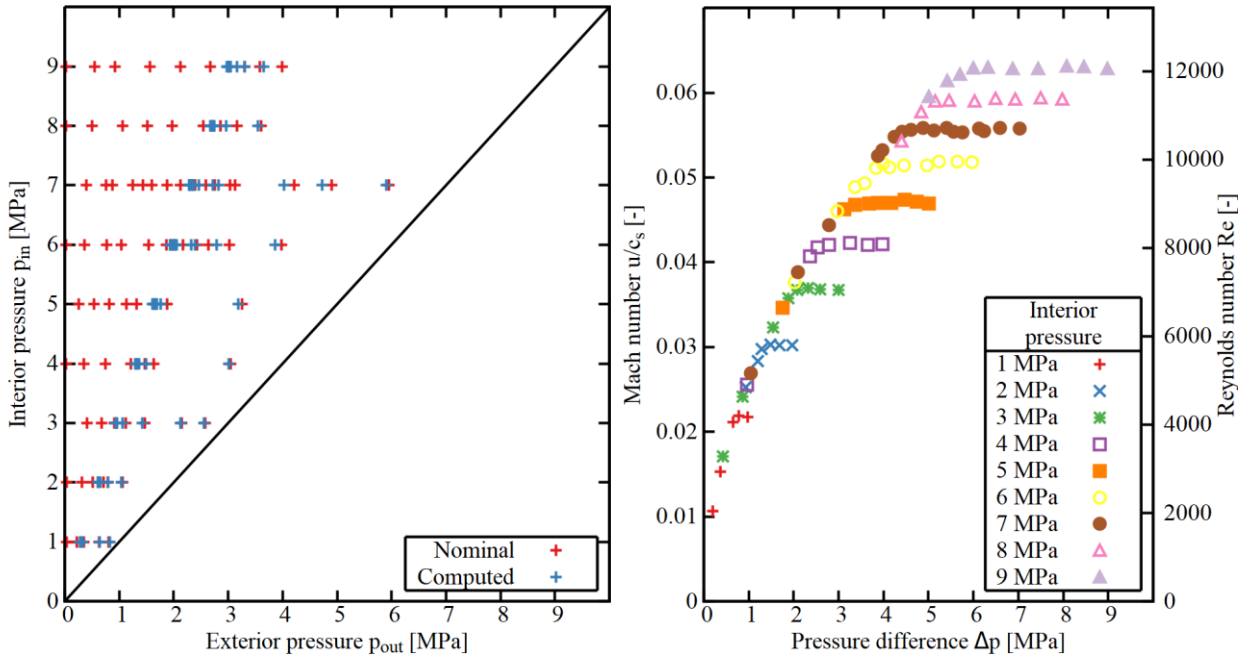

Figure 6. Analysis of the back pressure effect with the test Tube Slit 3 from Zhang et al. (2019)

This comparison indicates that, constant-density fluid assumed, the effective exit pressure is limited to a lower bound larger than the exit pressure, which depends on the interior pressure. The flow velocity is in the order of some percent of the sonic velocity, so it is far from critical conditions for liquid water. Also, the stagnation of the mass flow rate is not related to a specific Reynolds number, which indicates that no transient flow phenomenon seems to be responsible for the observed back pressure effect. Thus, the investigation of the back pressure effect remains at speculations – one of such idea would be the pressure-dependent solubility of nitrogen in cold liquid water: The depressurization would cause the nitrogen to bubble out, leading to a nitrogen-water mixture with lower density which could show critical flow phenomena due to the smaller sonic velocity of gaseous nitrogen. These thoughts underline that further

investigation of this topic is of importance, since it should have an effect on the assessment of the mass flow rates for operating SGT – none of the presented models is able to include the back pressure effect so far.

TIGHT CRACKS AND MORPHOLOGY

As a basic parametric study, axial and circumferential crack-like leaks in steam generator tubes are computed with the WinLeck computer program. The incompressible fluid model and the two-phase models are imposed. Based on Park et al. (2015), morphology parameters of a local roughness of 8 µm and a global roughness of 80 µm are assumed, with 1.1 global path deviations and 1.3 total path deviations, and a turn density of 8/mm. The estimation of COD and leak rate is shown in Figure 7.Two flow rate options are shown by the same color for each crack orientation; they are easy to distinguish since the single-phase computation yield higher flow rates than the two-phase computations.

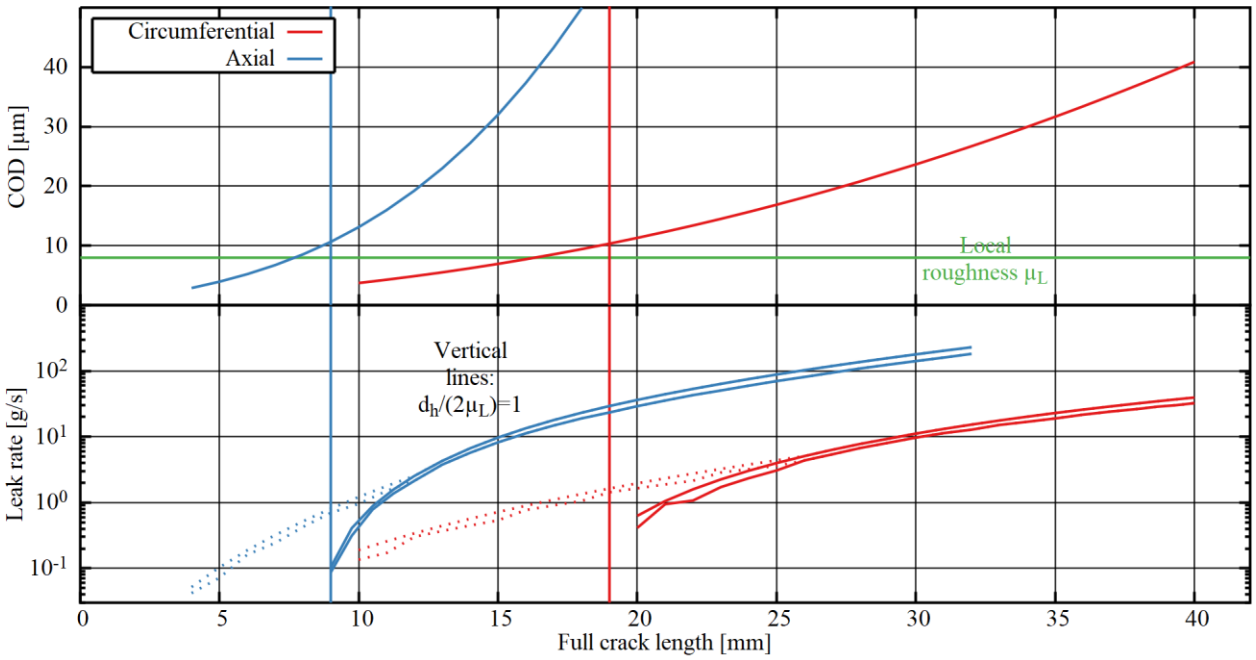

Figure 7. Leak rate as a function of crack length

Due to the hoop stresses, the axial cracks generally have a larger COD and consequently a higher mass flow rate than the circumferential cracks. The basic parametric study shows that leak rates in the order of few g/s, which would be a typical SGT leak detection level, correspond to COD values in the order of the local roughness. This regime is challenging to compute, and the friction factor in this regime is also very high. (Note that the friction factor is limited to 1 in for the dotted lines, whereas it is unlimited for the solid lines.)

As seen in the estimate of typical leak dimensions, the relevant leaks are very small and tight, and assuming a stress corrosion damage mechanism, the surface roughness of such a leak is easily in the order of magnitude of the crack width COD. The usual computational approach involves the improved morphology model by Paul et al. (1995). However, the actual number of leak rate experiments with stress corrosion cracks and significant morphology effects is rather small. Besides the two tests described by Kuppermann et al. (1983) and also by Chexal and Horowitz (1987), which are difficult to evaluate since the actual leak opening is not measured, only the test series by Collier et al. (1984) gives data points for

stress corrosion cracks at different openings. The flux density $G = \dot{m}/A$ as a function of the COD is shown in Figure 8.

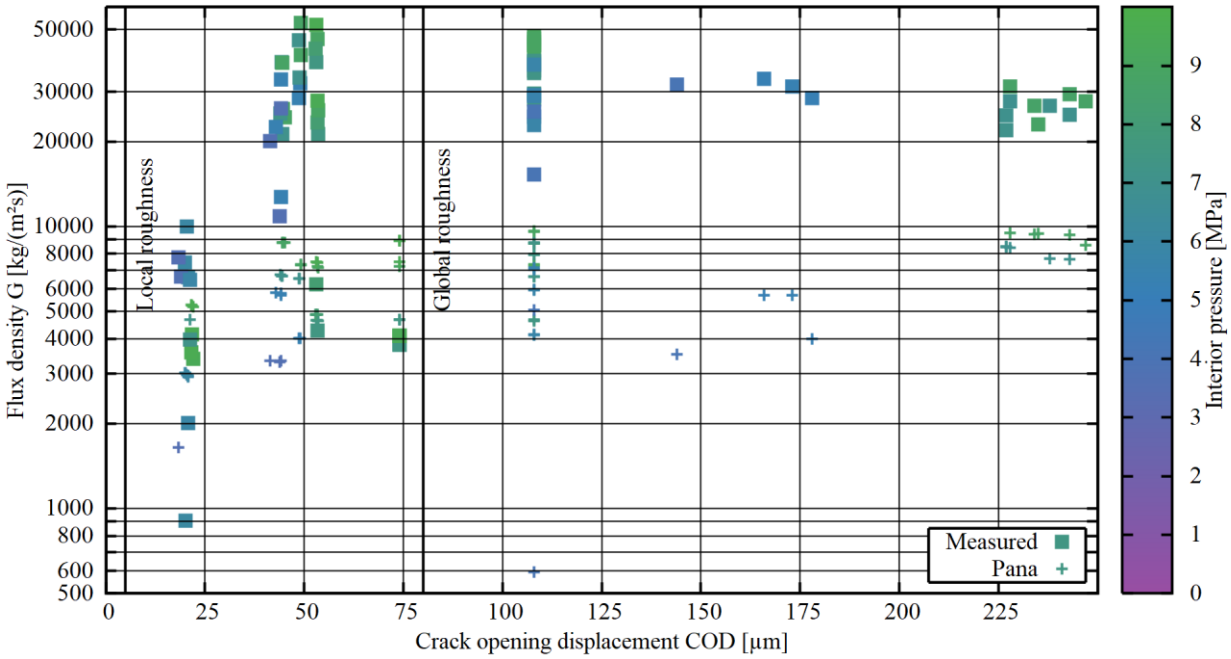

Figure 8. Stress corrosion crack with variating opening according to

The decrease in the flux G when COD approaches the local roughness is clearly visible, however, this is the only test reporting this effect for stress corrosion cracks and the absolute thickness is, with more than 20 mm, far from SGT conditions. This should motivate more experimental precision tests with COD-variable stress corrosion cracks, for an improved understanding of the morphology influence.

SUMMARY AND CONCLUSION

In this paper, three major aspects about SGT leaks are discussed. The first topic is the flow pattern and the flow rate computation, where three cases are discussed and compared with experimental observations. In the second topic, the back pressure effect is investigated shortly, while in the third topic, the relevance of morphology effects is highlighted.

One conclusion is that, thanks to the experimental and theoretical efforts in the last decade, a progress is made in understanding the flow pattern of gate-like leaks. Computational approaches such as the metastable jet assumption are able to model gate-like leak geometries adequately. However, there are indications that the role of the secondary side is more important than the theoretical models imply, which could be verified by additional tests with laboratory setups able to handle secondary side pressure. Also, the assessment of SGT leak detectability involves very tight cracks, where also the morphology influence is very important. The literature survey showed that leak rate data for stress corrosion cracks with controlled COD-variation is very limited. Additional measurements on stress corrosion leaks are therefore recommended.

ACKNOWLEDGEMENT

This work presented in this article funded by the German Federal Ministry for the Environment, Nature Conservation and Nuclear Safety (BMU), grants no. FKZ 4719R01326 and FKZ 4717R01370. Supplementary work was funded by the German Federal Ministry of Economic Affairs and Energy (BMWi), grant no RS1584. The authors thankfully acknowledge discussions within the international Tube Integrity Program (TIP-6), and with Craig Harrington (EPRI) concerning stress corrosion cracks.

REFERENCES

Chexal, B., Horowitz, J. (1983). "A critical flow model for flow through cracks in pipes," *24th ASME/AIChE National Heat Transfer Conference*, United States..

Collier, R. P., Stulen, F. B., Mayfield, M. E., Pape, D. B., Scott, P. M. (1984). *Two-Phase Flow Through Intergranular Stress Corrosion Cracks and Resulting Acoustic Emissions.* Report NP-3540-LD, Research Project T118-2, Electric Power Research Institute (EPRI), Columbus, Ohio, USA.

Fauske, H.K., Min, T.C. (1963). *A Study of the Flow of Saturated Freon-11 Through Apertures and Short Tubes*. Argonne National Laboratory, Report ANL-6667

Heckmann, K., Sievers, J. (2018). "Limits and Challenges of Leak-Before-Break," *8th International Conference & Workshop Quest for Energy (REMOO2018)*, May 2018, Venice, Italy

Heckmann, K., Silber, F., Sievers, J. Stumpfrock, L., Weihe, S. (2022). „A Metastable Jet Model for Leaks in Steam Generator Tubes," *Nuclear Engineering and Design*, 389, 11673. DOI: 10.1016/j.nucengdes.2022.111673

Kupperman, D., Shack, W. J., Claytor, T. (1983). "Leak Rate Measurements and Detection Systems," *CSNI Leak-Before-Break Conference*,

Liao, Y. and Lucas, D. (2021). "A review on numerical modelling of flashing flow with application to nuclear safety analysis," *Applied Thermal Engineering*, 182, 116002, 2021. DOI: 10.1016/j.applthermaleng.2020.116002

Majumdar, S., Bakhtiari, S., Kasza, K., Park, J. Y. (2001). *Validation of Failure and Leak Rate Correlations for Stress Corrosion Cracks in Steam Generator Tubes.* Argonne National Laboratory, Report NUREG/CR-6774 ANL-01/34

Pana, P., Müller, M. (1978). "Subcooled and two phase critical flow states and comparison with data," *Nuclear Engineering and Design*, 45, 117-125. DOI: 10.1016/0029-5493(78)90110-3

Park, J. H., Cho, Y. K., Kim, S. H., Lee, J. H. (2015). "Estimation of leak rate through circumferential cracks in pipes in nuclear power plants," *Nuclear Engineering and Technology*, 47, 332–339.

Paul, D. D., Ahmad, J., Scott, P. M., Flanigan, L. F., Wilkowski, G. M., 1995. *Evaluation and refinement of leak-rate estimation models.* Report NUREG/CR-5128-Rev.1, BMI-2164-Rev.1, Battelle, Columbus, Ohio. DOI: 10.2172/10165963

Revankar, S.T. und Riznic, J. (2019). "An experimental investigation of subcooled choked flow in actual steam generator tube cracks," *Nuclear Engineering and Design* 354, 110144. DOI: 10.1016/j.nucengdes.2019.06.006

Schmid, S., Silber, F.E., Heckmann, K., Kulenovic, R., Laurien, E., Sievers, J., Weihe, S. (2021). "Leak rate testing in the range of leak detection systems,"*Nuclear Engineering and Design*, 372, 111000. DOI: 10.1016/j.nucengdes.2020.111000

Silber, F.E., Stumpfrock, L. and Weihe, S. (2021)." Investigation on Leak Rates in Thin-Walled Structures," *ASME 2021 Pressure Vessels & Piping Conference*, Jul. 13 - 15, 2021, Virtual, Online. DOI: 10.1115/PVP2021-61955

Silber, F., Weihe, S., Heckmann, K., Sievers, J. (2022). „Specimen Testing for Steam Generator Tube Leaks With Measurement of Flow Patterns," *Transactions SMiRT-26*, Berlin/Potsdam, Germany.

Zaloudek, F.R. (1963). The critical flow of hot water through short tubes. U. S. Atomic Energy Commission (USAEC), Report HW-77594.

Zhang, K., You, H.B., Zhou, Y.K., Zhao, X.H., Zhang, J., Hou, Y.D., Tian, W.X., Su, G.H. und Qiu, S.Z. (2019). "Experimental investigations on leak flow rate characteristics of water through axial artificial microcracks of steam generator tubes under back pressure conditions," *Nuclear Engineering and Design*, 353, p. 110285. DOI: 10.1016/j.nucengdes.2019.110285

Zhang, K., Shi, Y.G., You, H.B., Zhao, X.H., Tian, W.X., Su, G.H., Qiu, S.Z. (2020). "Experimental study on leak flow rate characteristics of high pressure subcooled water through axial and circumferential microcracks of steam generator tubes under high back pressure conditions," *Annals of Nuclear Energy*, 145, 107551. DOI: 10.1016/j.anucene.2020.107551